DOI 10.1021/acs.nanolett.3c03345

Selective replacement of cholesterol with cationic amphiphilic drugs enables design of lipid nanoparticles with improved RNA delivery

Bram Bogaert[a], Aliona Debisschop[a], Thomas Ehouarne[a], Hannelore P. Van Eeckhoutte[b], Joyceline De Volder[b], An Jacobs[c], Eline Pottie[d], Riet De Rycke[e], Aurélie Crabbé[f], Pieter Mestdagh[g], Ine Lentacker[a], Guy G. Brusselle[b], Christophe Stove[d], Sandra Verstraelen[c], Tania Maes[b], Ken R. Bracke[b], Stefaan C. De Smedt[a], and Koen Raemdonck[a,]*

[a] Ghent Research Group on Nanomedicines, Laboratory of General Biochemistry and Physical Pharmacy, Faculty of Pharmaceutical Sciences, Ghent University, Ottergemsesteenweg 460, 9000 Ghent, Belgium

[b] Laboratory for Translational Research in Obstructive Pulmonary Diseases, Department of Respiratory Medicine, University Hospital Ghent, Ghent University, C. Heymanslaan 10, 9000 Ghent, Belgium

[c] Health Unit, Flemish Institute for Technological Research (VITO), Boeretang 200, 2400 Mol, Belgium

[d] Laboratory of Toxicology, Faculty of Pharmaceutical Sciences, Ghent University, Ottergemsesteenweg 460, 9000 Ghent, Belgium

[e] Ghent University Expertise Center for Transmission Electron Microscopy and VIB BioImaging Core, 9000 Ghent, Belgium

Department of Biomedical Molecular Biology, Ghent University, VIB Center for Inflammation Research, Ghent, Belgium

[f] Laboratory of Pharmaceutical Microbiology, Faculty of Pharmaceutical Sciences, Ghent University, Ottergemsesteenweg 460, 9000 Ghent, Belgium

[g] Department of Biomolecular Medicine, OncoRNAlab, C. Heymanslaan 10, Ghent University, 9000 Ghent, Belgium

[*] E-mail: koen.raemdonck@ugent.be

KEYWORDS: lipid nanoparticles, siRNA, mRNA, cationic amphiphilic drugs, drug repurposing, combination therapy, inhalation therapy, nebulization

TOC GRAPHIC:

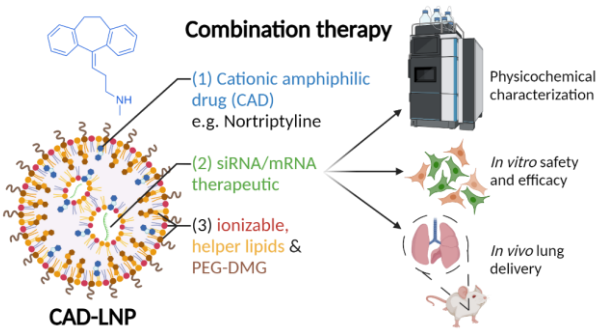

ABSTRACT: RNA delivery across biological barriers can be achieved by encapsulation in lipid nanoparticles (LNPs). Cationic amphiphilic drugs (CADs) are pharmacologically diverse compounds with ionizable lipid-like features. Here, we applied CADs as a fifth component into state-of-the-art LNPs via microfluidic mixing. Improved cytosolic delivery of both siRNA and mRNA was achieved by partly replacing the cholesterol fraction of LNPs by CADs. The LNPs could cross the mucus layer in a mucus-producing air-liquid interface model of human primary bronchial epithelial cells following nebulization. Moreover, CAD-LNPs demonstrated improved epithelial- and endothelial targeting following intranasal administration in mice, without marked pro-inflammatory signature. Importantly, a quantification of the CAD-LNP molar composition, as demonstrated for nortriptyline, revealed a gradual leakage of the CAD from the formulation during LNP dialysis. Altogether, these data suggest that the addition of a CAD prior to the rapid mixing process might have an impact on LNP composition, structure and performance.

The approval of the first RNA interference (RNAi)-based medicinal product Onpattro® (patisiran) in 2018 and the more recent clinical success of the SARS-CoV-2 messenger RNA (mRNA)-based vaccines (Comirnaty® and Spikevax®) underscore the potential of RNA-based drugs [1–4]. Small interfering RNAs (siRNAs) activate the cytosolic RNAi pathway to induce sequence-specific gene silencing, thereby expanding the range of druggable targets beyond what can be reached by conventional small molecules or monoclonal antibodies [5,6]. Alternatively, intracellular mRNA delivery can drive production of any protein of interest, with applications in vaccination and protein replacement therapy [7]. Lipid nanoparticles (LNPs) have become a well-established platform to package, protect and deliver various nucleic acid cargoes into the cytosol of cells. LNP formulations typically consist of four main lipid components, *i.e.* (i) an ionizable cationic lipid, (ii) a helper lipid such as the phospholipid 1,2-distearoyl-*sn*-

glycero-3-phosphocholine (DSPC), (iii) cholesterol and (iv) a polyethylene glycol (PEG)-lipid, each having a specific function. While the ionizable cationic lipids, *e.g.* DLin-MC3-DMA denoted as MC3 (Onpattro®), ALC-0315 (Comirnaty®) and SM-102 (SpikeVax®), are mainly responsible for nucleic acid encapsulation and cytosolic delivery through endosomal escape, the inclusion of helper lipids, cholesterol and PEG-lipids is essential to maintain membrane rigidity and LNP stability [8–12]. An alternative LNP composition, including a fifth component in conventional LNPs*, i.e*. an additional cationic, anionic, or ionizable lipid component, enabled selective organ targeting to lung, spleen and liver, respectively [13,14].

Despite recent advances in LNP design and manufacturing, only limited endosomal escape efficiencies (~1-4%) are reported for state-of-the-art LNPs [15–17]. In previous work, we have intensively investigated the potential of small molecules, more specifically cationic amphiphilic drugs (CADs), to enhance the intracellular delivery of small nucleic acids [18,19]. A variety of CADs (*e.g.* antihistamines, antidepressants and antihypertensives) was identified to promote cytosolic delivery of siRNA from endolysosomes through the transient induction of (phospho)lipidosis, lysosomal swelling and lysosomal membrane permeabilization (LMP) [20–22]. This acquired lysosomal storage disease phenotype results from the lysosomal accumulation of CADs where their membrane insertion leads to the functional inhibition of acid sphingomyelinase [20,21]. Exploiting their ability to integrate in lipid membranes, CADs have been more recently repurposed as both structural and pharmacologically functional components of lipid-based complexes termed CADosomes [23]. Self-assembly of lipid-like CADs with the helper lipid 1,2-dioleoyl-*sn*-glycero-3-phosphoethanolamine (DOPE) into positively charged vesicles enabled subsequent complexation and delivery of mRNA *in vitro* as well as *in vivo* following topical application to the cornea of rabbit eyes, providing opportunities for drug combination therapy [23]. However, this formulation strategy, applying a two-step complexation process with only DOPE as a lipid component, appeared less optimal

for siRNA delivery and is possibly less suited for other administration routes due to relatively low RNA encapsulation and thus exposure of the siRNA to degradation. Therefore, we aimed to expand this drug combination concept towards siRNA therapeutics by applying CADs as a fifth component into state-of-the-art LNPs produced *via* one step microfluidic mixing, further referred to as CAD-LNPs.

siRNA CAD-LNPs with reduced ionizable lipid content

The clinically approved Onpattro® formulation containing the ionizable lipid MC3, the helper lipids DSPC, cholesterol and DMG-PEG_{2000} in a 50:10:38.5:1.5 molar ratio, was initially selected to design CAD-LNPs by gradually changing the ionizable lipid-to-CAD ratio [1,4]. It is well known that CADs, especially tricyclic compounds (*e.g.* tricyclic antidepressants and antihistamines), are able to interact with lipid membranes through coulomb interactions or Van der Waals forces, changing lipid bilayer properties [24–26]. Therefore, the tricyclic antidepressant nortriptyline hydrochloride (NT) (clogP 4.51; pKa 10.1) was applied as model CAD compound to replace either 25 or 40 mol% of the MC3 fraction, respectively (**Figure 1a**). Stable MC3-NT (25:25) and MC3-NT (10:40) LNPs were obtained with >70% siRNA encapsulation efficiency and formulations remained stable after dialysis and storage in phosphate-buffered saline (PBS) at 4°C for at least 8 weeks (**Figure 1b-d**). The addition of a relatively low CAD fraction (MC3-NT (25:25)) substantially increased cellular uptake relative to the MC3 control, while the opposite was observed for the MC3-NT (10:40) LNPs (**Figure 1e**). However, in complete cell culture medium (CCM) the gene silencing efficiency in an eGFP-expressing H1299 cell model was still significantly higher for the MC3 LNPs (**Figure 1f-g**). Incubating MC3 and MC3-NT (25:25 and 10:40) LNPs in serum-free OptiMEM® drastically lowered both cellular uptake as well as gene silencing, indicating the need for serum proteins towards efficient cell transfection (**Figure S1**) [27,28]. Possibly, the adsorption of apolipoprotein E on the surface of the MC3 LNPs also stimulates low density lipoprotein receptor-mediated

internalization in H1299 cells, as described for hepatocytes [4,29]. Lastly, a CellTiter-Glo® cell viability assay demonstrated the absence of cytotoxicity for both MC3- and modified MC3-NT LNPs (**Figure S2a**). Altogether, partially replacing the ionizable lipid MC3 with the CAD molecule NT results in stable MC3-NT LNPs with acceptable siRNA encapsulation, albeit with marginally reduced transfection efficiency.

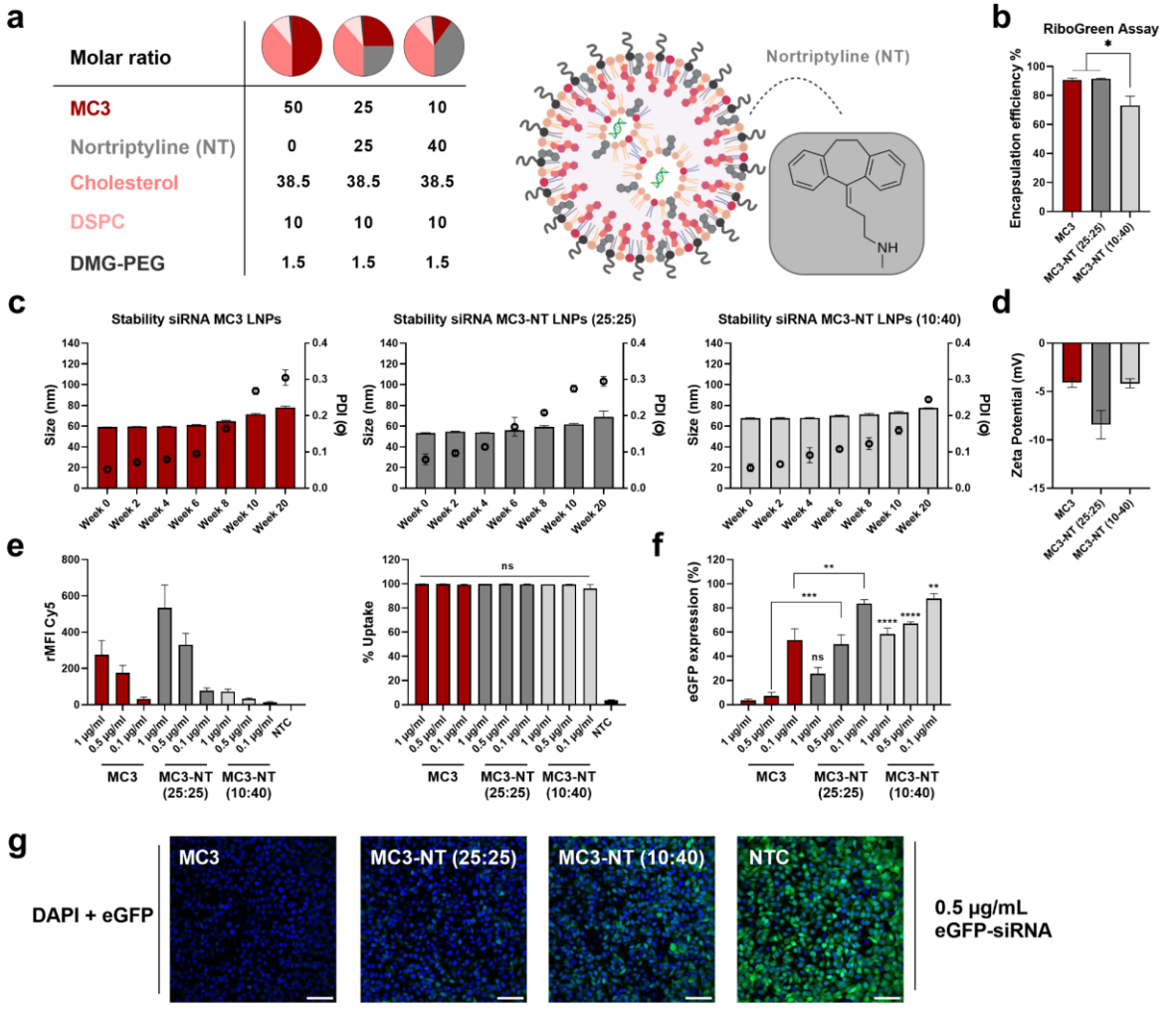

Figure 1. *Physicochemical properties and cytosolic siRNA delivery of siRNA-loaded CAD-LNPs with reduced ionizable lipid fraction.* ***(a)*** *Schematic illustration of the siRNA-loaded CAD-LNPs MC3-NT (25:25) and MC3-NT (10:40), produced by replacing the MC3 ionizable lipid fraction with the CAD nortriptyline hydrochloride (NT).* ***(b)*** *Encapsulation efficiency of siRNA as measured by the Quant-iT™ RiboGreen® RNA assay.* ***(c-d)*** *Dynamic light*

scattering data (hydrodynamic size (bars), polydispersity index (PDI; dots) and zeta potential) of MC3 and MC3-NT (25:25 – 10:40) LNPs. Stability was analyzed after dialysis and storage in PBS at 4°C up to twenty weeks after production. ***(e)*** *Cy5+ relative mean fluorescence intensity (rMFI, normalized to NTC), cellular uptake and* ***(f)*** *enhanced green fluorescent protein (eGFP) silencing of the LNPs in a H1299-eGFP lung epithelial cell line at different siRNA concentrations.* ***(g)*** *Representative confocal images of H1299-eGFP cells 48 h after transfection with anti-eGFP siRNA-loaded MC3 and MC3-NT LNPs, with nuclei (DAPI; blue) and eGFP expression (green). Scale bars correspond to 100 µm. Data are represented as mean ± the standard error of the mean (SEM) for three independent repeats (n=3). Statistical analysis was performed using One Way Anova with Tukey Correction (ns $p > 0.05$, * $p \leq 0.05$, ** $p \leq 0.01$, *** $p \leq 0.001$, **** $p \leq 0.0001$). NTC: non-treated control, CAD: cationic amphiphilic drug, LNP: lipid nanoparticle. Illustration created with BioRender.com.*

siRNA CAD-LNPs with reduced cholesterol content

Having established the importance of maintaining sufficiently high ionizable lipid fractions in the design of CAD-LNPs, we next sought to evaluate the influence of cholesterol. Most research groups have focused on modulating the ionizable lipid component to optimize *in vitro-in vivo* RNA delivery by LNPs [30–35]. However, the type and fraction of helper lipids such as cholesterol or phospholipids, albeit studied less extensively, can have a profound impact on RNA delivery efficiency [10,36–38]. Here, we designed CAD-LNPs by gradually replacing the tetracyclic cholesterol with mounting fractions of the tricyclic antidepressant NT while leaving the ionizable lipid fraction unchanged (**Figure 2a)**. Transmission electron microscopy (TEM) images of the MC3-NT (50:25) LNP, with 25 mol% cholesterol replaced with NT, revealed no marked difference in neither LNP morphology nor LNP size compared to the MC3 control formulation (**Figure 2b**). siRNA-loaded MC3-NT (50:10 – 50:25 – 50:38.5) LNPs show a

similar size range (~60-70 nm) and near-neutral zeta potential, comparable with the parent MC3 LNPs (**Figure 1 and Figure 2c-d**). Interestingly, replacing the cholesterol fraction again had a positive effect on LNP stability over time, decreasing the PDI values relative to the MC3-LNPs up to twenty weeks after production (**Figure 1 and Figure 2c**). In contrast, lowering cholesterol levels slightly reduced siRNA encapsulation efficiency (**Figure 2e**). As designing an LNP formulation combining both a CAD and a siRNA would be of interest for drug combination therapy, we next studied if the CAD molecule nortriptyline (NT) remained pharmacologically active after incorporation in cholesterol-reduced CAD-LNPs. Therefore, we investigated the antagonistic effect of NT at the 5-HT_{2A}R serotonin receptor. The employed assay consists of a HEK293T (Human Embryonic Kidney) cell line stably expressing the 5-HT_{2A}R and the cytosolic protein β-arrestin 2 (βarr2) in the Nanoluciferase Binary Technology (NanoBiT®) system as illustrated in **Figure 2f** [39–42]. As expected, the antagonist NT blocked the lysergic acid diethylamide (LSD) agonist-induced βarr2 recruitment in a dose-dependent manner, leading to impaired nanoluciferase complementation and a reduced luminescence signal. The MC3-NT (50:25) and MC3-NT (50:10) LNPs reduced 5-HT_{2A}R activation with an additional 39% and 33% respectively, compared to MC3 LNPs at the highest siRNA concentration (**Figure 2g**). The obtained real-time receptor activation profiles clearly indicate identical trends (**Figure S3**).

Nevertheless, the observed antagonistic effect in **Figure 2g** is ~6-fold lower than anticipated based on the theoretical NT concentration. Therefore, we quantified the MC3-NT (50:25) LNP composition as a function of dialysis time (Figure S4). It is shown that NT gradually diffuses out of the LNP during dialysis, with still ~15 mol% NT remaining in the formulation after 2 h dialysis (starting from a theoretical 25 mol%), while overnight dialysis (18 h) further reduces the NT molar fraction to ~1.5 mol%. These data could be explained by the relatively low lipophilicity of the compound (clogP ~4.5) compared to conventional ionizable lipids (reported

clogP ~ 15-20) [11]. The dose of the CAD that is maintained in the CAD-LNP formulation will thus highly depend on the dialysis time and will most likely be a combination of both free as well as LNP-integrated compound. Of note, it was verified that during the dialysis process, the encapsulation efficiency of the siRNA was unaffected (Figure S5). Overall, partly replacing the cholesterol fraction by the tricyclic CAD molecule NT demonstrated that stable MC3-NT LNPs could be formed with acceptable siRNA encapsulation and without impeding the pharmacological activity of the CAD maintained in the formulation.

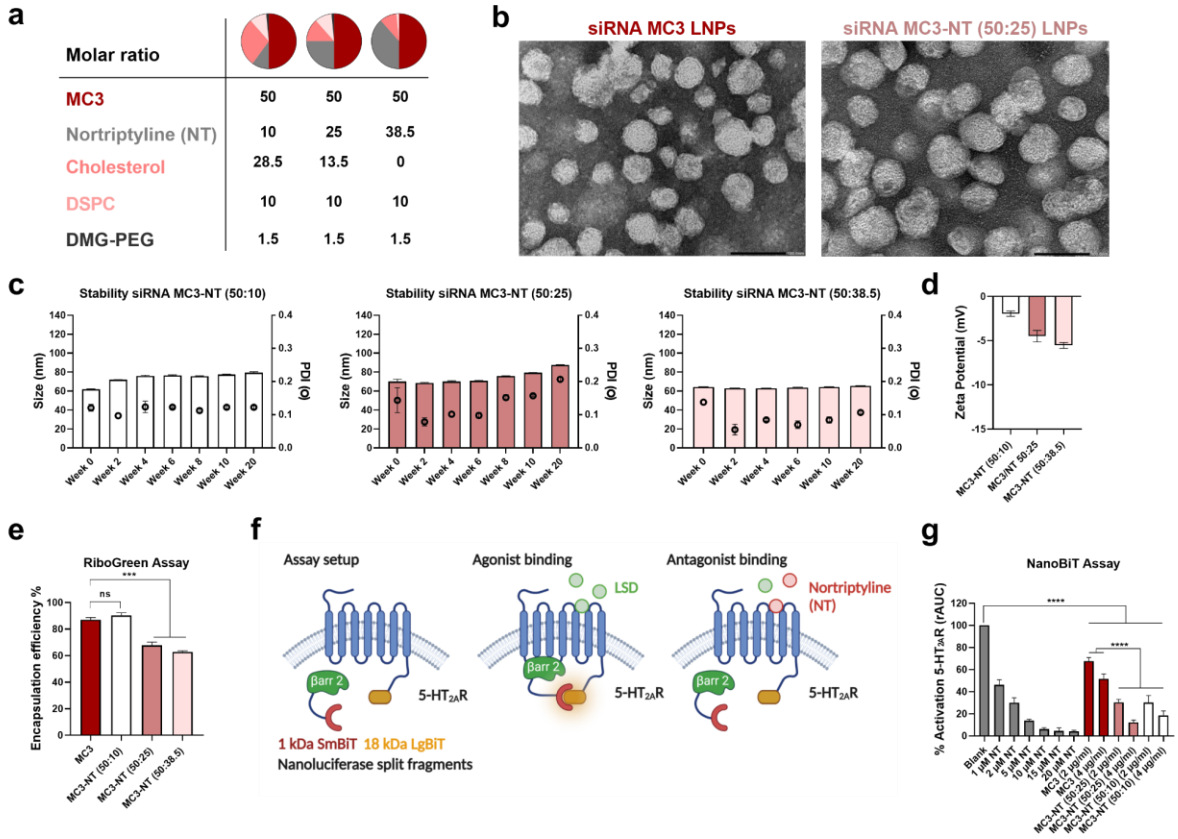

Figure 2. *Physicochemical properties and pharmacological activity of siRNA-loaded CAD-LNPs formulated with reduced cholesterol fraction.* ***(a)*** *Schematic overview of MC3-NT (50:10), MC3-NT (50:25) and MC3-NT (50:38.5) formulated by replacing part of the cholesterol fraction with nortriptyline hydrochloride (NT).* ***(b)*** *Representative transmission electron microscopy (TEM) image of siRNA MC3 and MC3-NT (50:25) LNPs. Scale bar*

corresponds to 100 nm. ***(c-d)*** *Dynamic light scattering data (hydrodynamic size, polydispersity index (PDI) and zeta potential) of MC3-NT (50:10 – 50:25 – 50:38.5) LNPs. Stability was analyzed after dialysis and storage in PBS at 4°C up to twenty weeks after production.* ***(e)*** *Encapsulation efficiency of siRNA as measured by the Quant-iT™ RiboGreen® RNA assay.* ***(f)*** *Schematic illustration of the NanoBiT® system, with HEK293T cells stably expressing two inactive luciferase split fragments (18 kDa LgBiT and 1 kDa SmBiT), coupled to the 5-HT_{2A}R (serotonin 2A receptor) and the cytosolic protein β-arrestin 2 (βarr2), respectively. Binding of a receptor agonist, in this case lysergic acid diethylamide (LSD), results in βarr2 recruitment to the 5-HT_{2A}R with the concomitant functional complementation of the enzyme, which can be monitored through luminescence read-out. Binding of a receptor antagonist, e.g. NT, inhibits LSD-induced βarr2 recruitment and subsequent luciferase complementation.* ***(g)*** *Percentage 5-HT_{2A}R activation induced by blank, NT dose range between 1-20 µM, MC3 LNPs and both MC3-NT (50:10 and 50:25) LNPs, measured by calculating the normalized area under the curve (rAUC) values of the receptor activation profiles. 10 nM LSD was added to all samples and luminescence was monitored continuously over 2 h. Data are represented as mean ± the standard error of the mean (SEM) for three independent repeats (n=3). Statistical analysis was performed using One Way Anova with Tukey Correction (*** $p \leq 0.001$, **** $p \leq 0.0001$). CAD: cationic amphiphilic drug, LNP: lipid nanoparticle. Illustration created with BioRender.com.*

In vitro transfection efficiency of cholesterol-reduced CAD-LNPs in pulmonary cell models

Currently, the liver is the organ of choice for systemic siRNA therapies. However, to broaden the therapeutic scope of siRNA, a great interest exists in delivering siRNA to extrahepatic tissues. The lung is an attractive target organ to apply RNA therapeutics for the treatment of lung-related pathologies. Unfortunately, inhalation therapy of RNA entails specific challenges

and currently no RNA-based product is clinically approved for administration *via* the inhaled route [43–45]. Here, our aim was to further investigate siRNA-loaded CAD-LNPs for local pulmonary delivery [46]. As stable MC3-NT LNPs with reduced cholesterol fraction could be formulated *via* microfluidic mixing, we next sought to evaluate their *in vitro* siRNA delivery efficiency in H1299-eGFP lung epithelial cells. No major difference in cellular internalization was observed between MC3 and both cholesterol reduced MC3-NT (50:10), MC3-NT (50:25) LNPs, except for the lowest siRNA dose (0.005 µg/ml). In contrast, MC3-NT (50:38.5) LNPs, which contain the highest initial NT fraction and are devoid of cholesterol, demonstrated impaired cellular uptake (**Figure 3a and Figure S6a**). Interestingly, despite significant loss of NT during dialysis (Figure S4), MC3-NT (50:25) LNPs (n>3) outperformed state-of-the-art MC3-LNPs (n=11) in terms of eGFP knockdown, requiring on average ~3-fold lower siRNA dose to reach the same level of gene silencing (**Figure 3b**), without inducing cytotoxicity (**Figure S2b**). In addition, despite a ~20-fold reduced intracellular siRNA dose (**Figure S6a**), MC3-NT (50:38.5) LNPs still maintained comparable knockdown efficiency as MC3 LNPs. One possible explanation for these observations could be that the relatively low fraction of NT remaining in the CAD-LNP formulation induces endolysosomal swelling and LMP after CAD-LNP endocytosis and trafficking towards the lysosomal compartment, which could stimulate cytosolic siRNA release [18–21]. However, this hypothesis could not be confirmed as transfection with MC3-NT (50:25) did not result in a significant increase in the total (endo)lysosomal volume and cellular granularity, which are hallmarks of the CAD-induced lysosomal phenotype (**Figure S7**) [18–21]. Moreover, earlier work from our group indicated that CADs cannot promote siRNA delivery by LNPs, most likely because the nucleic acid is tightly complexed by the ionizable lipids within the LNP core, and is not available for escape through the CAD-induced pores in the lysosomal membrane [20]. Of note, merely reducing the cholesterol fraction in MC3 LNPs without NT addition did not enhance eGFP silencing (**Figure S8**).

Likewise, spiking MC3-LNPs with 25 mol% NT while equally lowering the molar fractions of all other LNP components did not improve cytosolic siRNA delivery (**Figure S8**). Moreover, we could also confirm the higher eGFP knockdown of the MC3-NT (50:25) LNPs relative to the parent MC3-LNPs in a HT1080-eGFP fibrosarcoma cell line (**Figure S6b**). Additionally, mRNA-loaded MC3-NT (50:25) LNPs outperformed MC3-LNPs in a HeLa cell line with similar ~3-fold increase in rMFI values at the highest mRNA concentration (**Figure S9**). Taking into account the gradual leakage of the NT compound from the CAD-LNPs, the improved RNA delivery compared to the unmodified LNPs can possibly be influenced by (1) the variation in molecular composition of the LNPs due to NT addition, (2) a difference in CAD-LNP nanoarchitecture by the presence of NT during the microfluidic mixing process and/or (3) a change in LNP properties due to the remaining NT fraction. A more detailed assessment will be required to further elucidate the biophysical and physicochemical parameters involved in these observations.

To evaluate the potential of the developed CAD-LNPs for inhalation therapy with siRNA drugs, MC3- and MC3-NT (50:25) LNP delivery was investigated in a mucus-producing air-liquid interface (ALI) model of human primary bronchial epithelial cells (MucilAir™), using nebulization to deposit the LNPs on the cells. Importantly, the hydrodynamic size of both LNPs remained intact after nebulization using the VITROCELL® Cloud 12 system, equipped with an Aerogen® Pro nebulizer, creating aerosol droplets with an aerodynamic diameter between 1-5 µm (**Figure 3c**). This observation is in contrast with other literature reports showing an increased hydrodynamic size of mRNA-loaded LNPs post-nebulization [47,48]. One of the most important extracellular physiological barriers for inhaled nanomedicines is the mucus layer that lines the bronchial epithelium [49,50]. To evaluate the impact of mucus, we quantified the cellular internalization of Cy5-siRNA loaded MC3-NT (50:25) and MC3-LNPs with equal siRNA dose (0.5 µg/mL) 24 h post-nebulization on the MucilAir™ ALI culture (**Figure 3d**). On average

~50% Cy5+ bronchial epithelial cells were reached by both MC3 and MC3-NT (50:25) LNPs. This indicates that a substantial fraction of the nebulized LNPs can cross the mucus layer to interact with the underlying epithelial cells. The mucus mesh network has a reported average pore size between 100 and 200 nm [49,51], which exceeds the hydrodynamic diameter of the siRNA-loaded LNPs post-nebulization. Nevertheless, confocal imaging also clearly revealed the presence of LNPs layered on top of the epithelial cell surface, possibly as a result of mucus entrapment (**Figure 3f**). Additionally, the beating frequency of the MucilAir™ ciliated cells (CBF) as well as the transepithelial electrical resistance (TEER), indicators of mucociliary clearance function and the cellular barrier integrity, respectively, were not significantly changed after LNP exposure (**Figure 3e, Figure S10**). A lactate dehydrogenase (LDH) assay confirmed the absence of cytotoxicity after MC3-NT (50:25) LNP nebulization on the MucilAir™ ALI culture (**Figure S10**). To summarize, nebulized MC3-NT CAD-LNPs can cross the mucus barrier to reach (mucus-producing) primary bronchial epithelial cells.

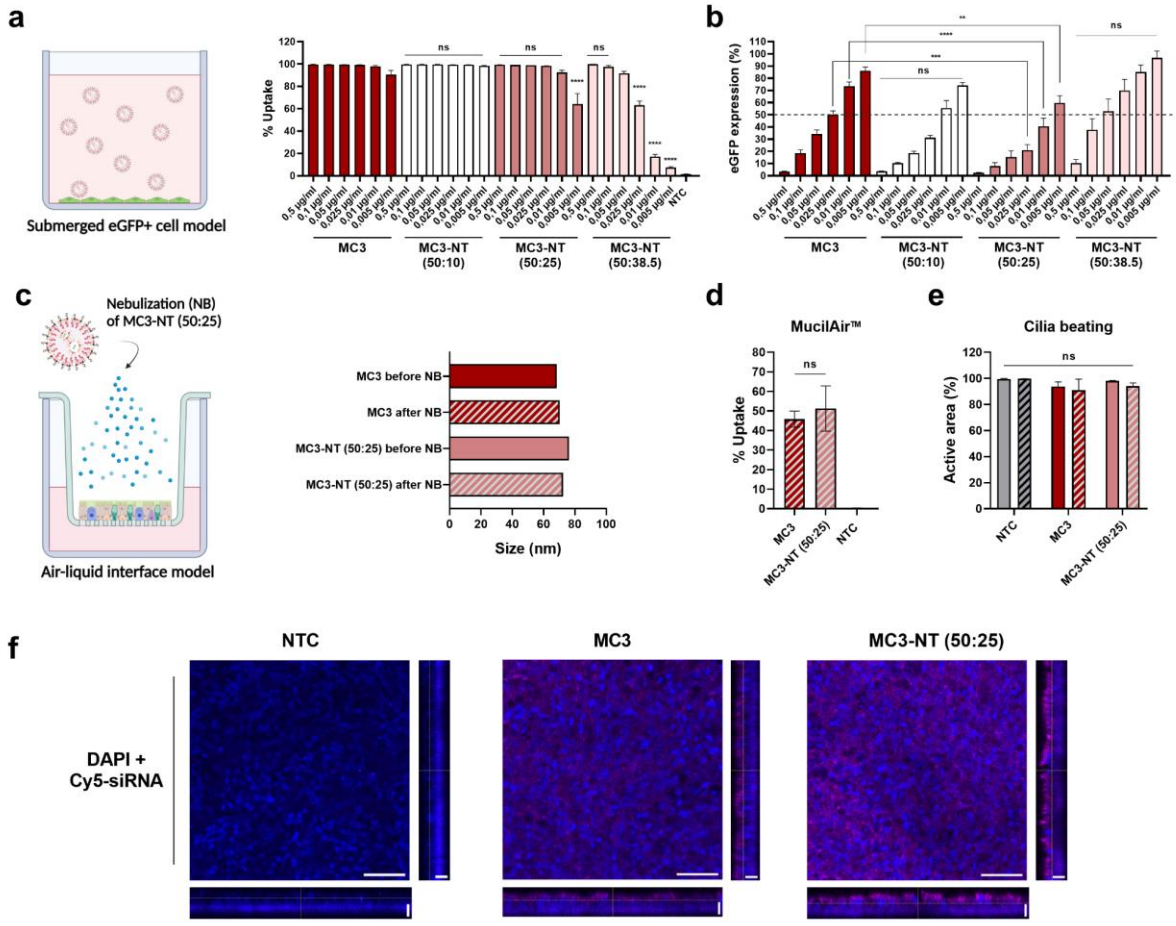

Figure 3. *Evaluating siRNA CAD-LNPs for cytosolic delivery in a submerged H1299-eGFP cell line and mucus crossing in a human air-liquid interface bronchial epithelial cell model.* ***(a)*** *Cellular uptake and* ***(b)*** *enhanced green fluorescent protein (eGFP) silencing of MC3-NT (50:10 – 50:25 – 50:38.5) LNPs in a submerged H1299-eGFP lung epithelial cell line at different siRNA concentrations.* ***(c-d)*** *Evaluating the impact of nebulization (NB) on Cy5-siRNA MC3-NT (50:25) and MC3-LNP delivery in an air-liquid interface (ALI) model using human primary bronchial epithelial cells (MucilAir™ Epithelix). Hydrodynamic size of LNPs was unaffected by nebulization, while a substantial fraction of LNPs are able to cross the mesh network of the mucus gel layer.* ***(e)*** *The cilia beating of epithelial cells was not influenced after LNP exposure.* ***(f)*** *Representative orthogonal confocal images of MucilAir™ tissue fixed 24 h after transfection with Cy5-siRNA (magenta) encapsulated in MC3-NT (50:25) and MC3-LNPs. Cell nuclei were stained with DAPI (blue). Scale bars correspond to*

*100 µm (XY) and 15 µm (XZ-YZ). Data are represented as mean ± the standard error of the mean (SEM) for minimum three independent repeats (n≥3). Statistical analysis was performed using One Way Anova with Tukey Correction (ns $p > 0.05$, * $p \leq 0.05$, ** $p \leq 0.01$, *** $p \leq 0.001$, **** $p \leq 0.0001$). CAD: cationic amphiphilic drug, LNP: lipid nanoparticle, NT: nortriptyline. Illustrations created with BioRender.com.*

Cholesterol-reduced siRNA CAD-LNPs with different CADs

Next, we evaluated a selection of other CADs with diverging physicochemical properties for siRNA CAD-LNP formation by replacing part of the cholesterol fraction. Also for these CADs, having a substantially lower clogP compared to state-of-the-art ionizable lipids, gradual diffusion out of the LNP formulation is hypothesized. Besides NT, a typical CAD with an aromatic tricyclic domain substituted with a secondary amine group, also an antihistamine with a heterocyclic amine piperidine was investigated (*i.e.* desloratadine, DES)[18,20,52] (clogP 3.97; pKa 9.73), as well as antidepressant CADs with monocyclic domains (*i.e.* fluoxetine, Fluox and fluvoxamine, Fluv) of which the latter contains a primary amine group (clogP 4.17 and 2.89; pKa 9.8 and 8.86) (**Figure 4a)**. Despite Fluv being the least hydrophobic compound tested, the siRNA encapsulation efficiency measured after microfluidic production and overnight dialysis of cholesterol-reduced MC3-Fluv (50:25) was >90%, while MC3-Fluox (50:25) reached almost 60%, comparable to MC3-NT (50:25) LNPs. Although DES resembles the chemical structure of NT most closely, MC3-DES (50:25) LNPs did not encapsulate siRNA well, showing <25% encapsulation efficiency (**Figure 4b**). As mentioned above, despite the anticipated transient integration of the CADs in the LNPs, these data suggest a strong impact of the applied CAD on the final LNP properties after dialysis. The hydrodynamic diameter of MC3-Fluv (50:25) and MC3-Fluox (50:25) remained stable ~70 nm with low PDI values (< 0.2) up to 20 weeks after formulation, stored in PBS at 4°C. Zeta potential values were again close to neutral, comparable to MC3 parent LNPs (**Figure 4c-d**). In contrast to MC3-NT

(50:25), significantly lower cellular uptake was observed in H1299-eGFP cells for both MC3-Fluv (50:25) and MC3-Fluox (50:25) LNPs, but the reduced percentage was most outspoken for MC3-DES (50:25) LNPs (**Figure 4e**). Nevertheless, eGFP silencing was still marginally improved for both MC3-Fluv (50:25) and MC3-Fluox (50:25) LNPs relative to MC3-LNPs, albeit less extensively as MC3-NT (50:25) LNPs (**Figure 3b and Figure 4f**). Altogether, these findings demonstrate that CADs with distinct chemical structure are useful for the design of CAD-LNPs, illustrating the broader applicability of such formulations and enabling drug combination therapy for a variety of diseases.

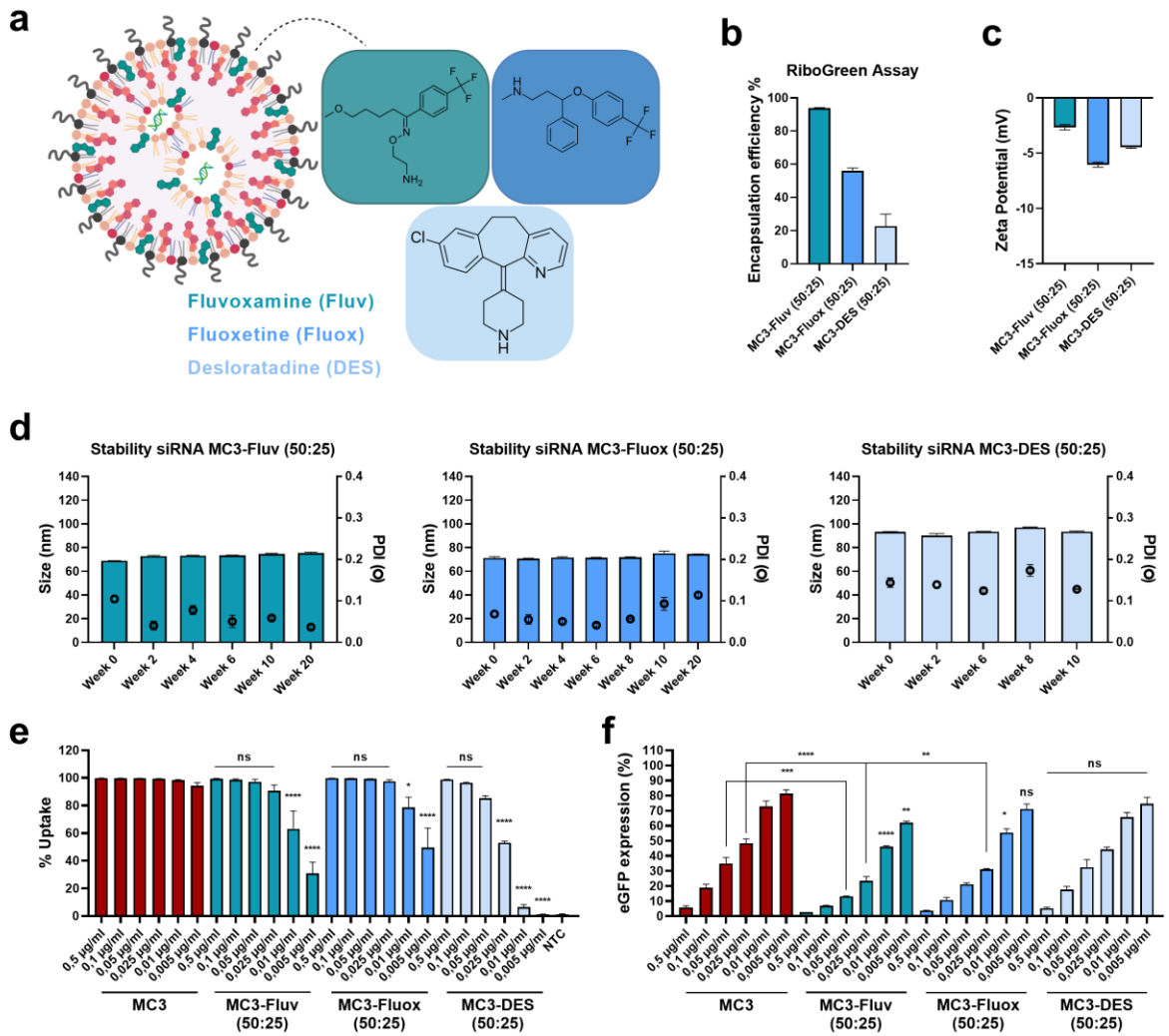

Figure 4. *Screening different CAD molecules for siRNA CAD-LNP formation and cytosolic delivery in a H1299-eGFP cell line.* ***(a)*** *Schematic illustration of the selected CAD molecules,*

fluvoxamine (Fluv), fluoxetine (Fluox) and desloratadine (DES) with different molecular structure to form siRNA-loaded CAD-LNPs with reduced cholesterol fraction. ***(b)*** *Encapsulation efficiency of siRNA-eGFP MC3-Fluv, MC3-Fluox and MC3-DES (50:25) LNPs, measured by the Quant-iT™ RiboGreen® RNA assay.* ***(c-d)*** *Dynamic light scattering data (hydrodynamic size, polydispersity index (PDI) and zeta potential) of MC3-Fluv, MC3-Fluox and MC3-DES (50:25) LNPs. Stability was analyzed after dialysis and storage in PBS at 4°C up to 10 or 20 weeks after production.* ***(e)*** *Cellular uptake and* ***(f)*** *enhanced green fluorescent protein (eGFP) silencing of the MC3-Fluv, MC3-Fluox and MC3-DES (50:25) LNPs in a H1299-eGFP lung epithelial cell line at different siRNA concentrations. siRNA-eGFP MC3-Fluv and MC3-Fluox (50:25) outperformed the state-of-the-art MC3 LNPs in eGFP knockdown efficiency, while no significant difference was observed for MC3-DES (50:25). Data are represented as mean ± the standard error of the mean (SEM) for minimum three independent repeats (n≥3). Statistical analysis was performed using One Way Anova with Tukey Correction (ns $p > 0.05$, * $p \leq 0.05$, ** $p \leq 0.01$, *** $p \leq 0.001$, **** $p \leq 0.0001$). CAD: cationic amphiphilic drug, LNP: lipid nanoparticle. Illustration created with BioRender.com.*

In vivo biodistribution and toxicity of siRNA CAD-LNPs following intranasal administration

Next, we investigated which pulmonary cell types could be reached with cholesterol-reduced MC3-NT and MC3-Fluox (50:25) LNPs following intranasal administration in mice (**Figure 5a**) and if differences could be observed with the parent MC3 LNPs. Macrophages were the most abundant cell type present in bronchoalveolar lavage (BAL) fluid (**Figure S11**) and both macrophages and neutrophils scavenged most of the Cy5-siRNA LNPs within 24 h post-administration in C57BL/6 mice (**Figure 5b**). The MFI values of Cy5+ macrophages were significantly higher compared to other immune cells in BAL such as neutrophils, DCs and

eosinophils, but decreased again after 48 h (**Figure S11**). Alveolar macrophages represent the largest cellular fraction in the alveoli and are mainly responsible for phagocytic clearance of foreign material [53]. The hydrodynamic size of LNPs is one of the major factors that influences macrophage uptake, with smaller particles (<200 nm) normally being less prone to macrophage clearance compared to their larger counterparts [54–56]. Interestingly, in lung tissue, MC3-NT (50:25) and especially MC3-Fluox (50:25) LNPs reached the pulmonary epithelium and endothelium significantly better compared to non-modified MC3 LNPs (**Figure 5c**). Although the percentage of Cy5+ epithelial cells decreased at later time points, the intracellular Cy5-siRNA dose remained significantly higher (>2-fold) compared to MC3 LNPs (**Figure 5c**). Of note, the resident macrophages present in the pulmonary tissue were reached to the same extent as in BAL, resulting in >60% Cy5+ macrophages at the 24 h time point (**Figure 5c, Figure S12**). Histological lung sections confirmed the presence of Cy5-siRNA in the pulmonary epithelial tissue for all LNPs tested (**Figure 5d, Figure S13**). Cy5 fluorescence was most prominent in the bronchial epithelium for MC3-LNPs and MC3-Fluox (50:25) LNPs 24 h post-administration, while after 48 h the MC3-NT (50:25) and MC3-Fluox (50:25) LNPs clearly showed the highest signal, confirming flow cytometry results.

Lastly, the levels of 13 inflammatory cytokines were quantified in the BAL fluid of C57BL/6 mice following intranasal LNP administration, using a LEGENDplex™ ELISA. Compared to PBS control, besides sporadic outliers, no relevant differences could be observed for IL-23, IL-1α, INF-γ, IL-12p70, IL-1β, IL-10, IL-27, IL-17A, IFN-β and GM-CSF (**Figure S14**). Only one cytokine, *i.e.* monocyte chemoattractant protein-1 (MCP-1), showed significantly higher levels 24 h post-administration for MC3-LNPs compared to PBS (* $p \leq 0.05$), which were reduced again for MC3-NT and MC3-Fluox LNPs. This chemokine plays an important role in the migration and infiltration of monocytes/macrophages [57]. Also for the pro-inflammatory cytokines TNFα and IL-6, the incorporation of NT and Fluox CADs into MC3-LNPs shows a

trend towards decreased levels compared to the parent LNPs, albeit not reaching statistical significance. A similar decreased pro-inflammatory effect of the CAD-modified LNPs was observed in the reduction of infiltrating neutrophils in BAL, albeit that MC3-Fluox (50:25) LNPs seem to stimulate eosinophilic influx at the 48 h time point (**Figure S15**). Altogether, this data indicate that intranasal administration of both state-of-the-art MC3-LNPs and modified CAD-LNPs did not induce marked pro-inflammatory effects.

In summary, a top-down approach was implemented to modify state-of-the-art MC3-LNPs (Onpattro®) with cationic amphiphilic drugs (CADs). CAD-LNPs were designed using CADs with diverging chemical structure and pharmacological properties, *i.e.* nortriptyline (NT), fluvoxamine (Fluv), fluoxetine (Fluox) and desloratadine (DES). Stable CAD-LNPs could be formed with conventional physicochemical properties and diverging siRNA encapsulation efficiencies, dependent on the selected CAD. Partially replacing the cholesterol fraction of parent MC3-LNPs with CADs resulted in an increased cytosolic siRNA delivery in human non-small cell lung carcinoma cells (H1299) while the opposite was observed for ionizable lipid substitution. Importantly, also mRNA delivery was significantly improved for the NT-modified LNPs, which demonstrates the applicability of this LNP platform towards larger RNA cargoes. Moreover, the pharmacological activity of the CAD was maintained after incorporation in the cholesterol-reduced CAD-LNPs, providing opportunities for drug combination therapy. Finally, we aimed to probe the value of the CAD-LNP platform for inhalation therapy. MC3-NT LNPs were able to cross the mucus layer following nebulization on a human primary mucus-producing air-liquid interface (ALI) bronchial tissue model to reach the underlying epithelial cells, which remains a major hurdle for pulmonary administration of RNA drugs. Furthermore, we demonstrated that intranasal administration in mice of MC3-NT and especially MC3-Fluox LNPs could deliver significantly higher siRNA doses to the pulmonary epithelium and endothelium compared to non-modified MC3-LNPs.

We could verify that intranasal administration of MC3-NT and MC3-Fluox LNPs in mice did not induce marked pro-inflammatory responses. Importantly, the abovementioned results were obtained with CAD-LNPs subjected to overnight dialysis, for which it was shown that the majority of the CAD (as demonstrated for NT) was removed from the original formulation. This gradual leakage of the CAD compound alters the molar lipid composition of the LNPs as a function of dialysis time. These data also suggest that the addition of a CAD prior to the rapid mixing process might have an impact on LNP formation, RNA encapsulation and biological performance. More detailed CAD-and LNP-specific studies will be required to further elucidate the critical LNP attributes affected by this process. Overall, this study demonstrates CAD-LNPs as a stable RNA delivery platform with applications in drug combination regimens for the treatment of various pathologies, including respiratory diseases. On the other hand, to increase drug retention in the LNPs, more hydrophobic CADs or lipid-modified CAD prodrugs might be considered in future work.

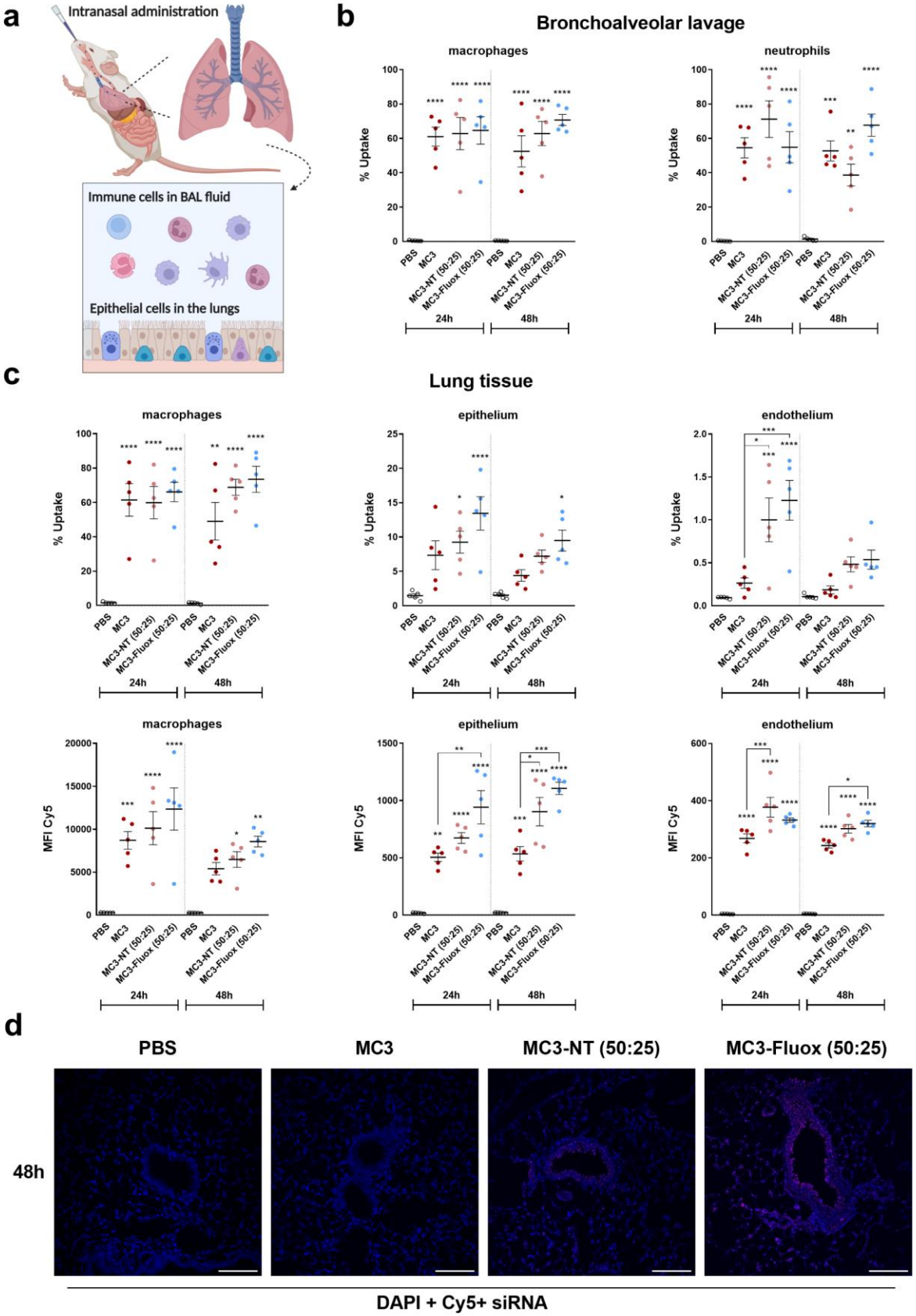

(caption on the next page)

Figure 5. *In vivo biodistribution of Cy5-siRNA loaded CAD-LNPs analyzed 24 h and 48 h after intranasal administration to C57BL/6 mice.* ***(a)*** *Schematic illustration of the in vivo biodistribution procedure.* ***(b)*** *Cellular uptake of Cy5-siRNA MC3, MC3-NT (50:25) and MC3-Fluox (50:25) LNPs in macrophages and neutrophils, as measured via flow cytometry after bronchoalveolar lavage (BAL).* ***(c)*** *Flow cytometric analysis of macrophages, epithelial - and endothelial cells of a single cell digest of the lung tissue.* ***(d)*** *Histological sections of the left lung were fixed and treated with DAPI to visualize the nuclei (blue) prior to confocal microscopy analysis to assess Cy5-siRNA (magenta) fluorescence. Per condition, one representative image of a series of n=4 analyzed images is shown. Scale bars correspond to 100 µm. All mice received a fixed Cy5-siRNA dose of 10 µg intranasally. Data are represented as mean ± the standard error of the mean (SEM) (n=5). Statistical analysis was performed using One Way Anova with Tukey Correction (* $p \leq 0.05$, ** $p \leq 0.01$, *** $p \leq 0.001$, **** $p \leq 0.0001$). CAD: cationic amphiphilic drug, LNP: lipid nanoparticle, NT: notriptyline, Fluox: fluoxetine. Illustration created with BioRender.com.*

ASSOCIATED CONTENT

Supporting Information. The Supporting Information is available free of charge online. Figures S1-15 describe additional experiments on the *in vitro* and *in vivo* physicochemical and biological properties of CAD-LNPs. Supporting Materials and Methods provide a detailed explanation on experiments, materials and methodology.

AUTHOR INFORMATION

Corresponding Author

* Koen Raemdonck - Ghent Research Group on Nanomedicines, Laboratory of General Biochemistry and Physical Pharmacy, Faculty of Pharmaceutical Sciences, Ghent University, Ottergemsesteenweg 460, 9000 Ghent, Belgium; Phone: +32 9 264 80 78; E-mail: Koen.Raemdonck@UGent.be

Author Contributions

The manuscript was written through contributions of all authors. All authors have approved the final version of the manuscript.

Notes

The authors declare no competing financial interests.

ACKNOWLEDGMENT

B. Bogaert is a doctoral fellow of the Research Foundation-Flanders (1S75019N, FWO, Belgium). K. Raemdonck additionally acknowledges the FWO for funding through research grant G039419N. K. Raemdonck has received funding from the European Research Council (ERC) under the European Union's Horizon 2020 research and innovation programme (Grant agreement No. 101002571, RESPIRNA). Financial support from the Ghent University Special Research Fund is gratefully acknowledged (BOF12/GOA/014, BOF19/GOA/008). J. De Volder is supported by FWO project G041819N. T. Maes is funded by FWO project G0G2318N and holds a Chiesi chair on environmental factors in asthma and a GSK chair on eosinophilic airway diseases. The authors thank the Centre for Advanced Light Microscopy at

Ghent University (Belgium) for the use and support of microscopy experiments, the Laboratory of Toxicology at Ghent University (Belgium) for the use of the NanoBiT® Assay, VITO Health Unit for the MucilAir™ (Epithelix) nebulization experiments and the Department of Respiratory Medicine at the University Hospital of Ghent for the collaboration on the *in vivo* biodistribution study.

REFERENCES

1. Akinc, A. *et al.* The Onpattro story and the clinical translation of nanomedicines containing nucleic acid-based drugs. *Nat Nanotechnol* **14**, 1084–1087 (2019).

2. Polack, F. P. *et al.* Safety and efficacy of the BNT162b2 mRNA Covid-19 vaccine. *New England Journal of Medicine* **383**, 2603–2615 (2020).

3. Baden, L. R. *et al.* Efficacy and safety of the mRNA-1273 SARS-CoV-2 vaccine. *New England Journal of Medicine* **384**, 403–416 (2021).

4. Kulkarni, J. A., Witzigmann, D., Chen, S., Cullis, P. R. & van der Meel, R. Lipid Nanoparticle Technology for Clinical Translation of siRNA Therapeutics. *Acc Chem Res* **52**, 2435–2444 (2019).

5. Whitehead, K. A., Langer, R. & Anderson, D. G. Knocking down barriers: Advances in siRNA delivery. *Nat Rev Drug Discov* **8**, 129–138 (2009).

6. Wittrup, A. & Lieberman, J. Knocking down disease: a progress report on siRNA therapeutics. *Nat Rev Genet* **16**, 543–552 (2015).

7. Hou, X., Zaks, T., Langer, R. & Dong, Y. Lipid nanoparticles for mRNA delivery. *Nat Rev Mater* **6**, 1078–1094 (2021).

8. Rietwyk, S. & Peer, D. Next-Generation Lipids in RNA Interference Therapeutics. *ACS Nano* **11**, 7572–7586 (2017).

9. Hald Albertsen, C. *et al.* The role of lipid components in lipid nanoparticles for vaccines and gene therapy. *Adv Drug Deliv Rev* **188**, 114416 (2022).

10. Kulkarni, J. A., Witzigmann, D., Leung, J., Tam, Y. Y. C. & Cullis, P. R. On the role of helper lipids in lipid nanoparticle formulations of siRNA. *Nanoscale* **11**, 21733–21739 (2019).

11. Eygeris, Y., Gupta, M., Kim, J. & Sahay, G. Chemistry of Lipid Nanoparticles for RNA Delivery. *Acc Chem Res* **55**, 2–12 (2022).

12. Suzuki, T. *et al.* PEG shedding-rate-dependent blood clearance of PEGylated lipid nanoparticles in mice: Faster PEG shedding attenuates anti-PEG IgM production. *Int J Pharm* **588**, 119792 (2020).

13. Cheng, Q. *et al.* Selective organ targeting (SORT) nanoparticles for tissue-specific mRNA delivery and CRISPR–Cas gene editing. *Nat Nanotechnol* **15**, 313–320 (2020).

14. Dilliard, S. A., Cheng, Q. & Siegwart, D. J. On the mechanism of tissue-specific mRNA delivery by selective organ targeting nanoparticles. *Proceedings of the National Academy of Sciences* **118**, e2109256118 (2021).

15. Stewart, M. P., Langer, R. & Jensen, K. F. Intracellular delivery by membrane disruption: Mechanisms, strategies, and concepts. *Chem Rev* **118**, 7409–7531 (2018).

16. Stewart, M. P., Lorenz, A., Dahlman, J. & Sahay, G. Challenges in carrier-mediated intracellular delivery: Moving beyond endosomal barriers. *Wiley Interdiscip Rev Nanomed Nanobiotechnol* **8**, 465–478 (2016).

17. Liu, S. *et al.* Membrane-destabilizing ionizable phospholipids for organ-selective mRNA delivery and CRISPR–Cas gene editing. *Nat Mater* **20**, 701–710 (2021).

18. Joris, F. *et al.* Repurposing cationic amphiphilic drugs as adjuvants to induce lysosomal siRNA escape in nanogel transfected cells. *Journal of Controlled Release* **269**, 266–276 (2018).

19. Joris, F., De Smedt, S. C. & Raemdonck, K. Small molecules convey big messages: Boosting non-viral nucleic acid delivery with low molecular weight drugs. *Nano Today* **16**, 14–29 (2017).

20. Van de Vyver, T. *et al.* Cationic Amphiphilic Drugs Boost the Lysosomal Escape of Small Nucleic Acid Therapeutics in a Nanocarrier-Dependent Manner. *ACS Nano* **14**, 4774–4791 (2020).

21. Van de Vyver, T., De Smedt, S. C. & Raemdonck, K. Modulating intracellular pathways to improve non-viral delivery of RNA therapeutics. *Adv Drug Deliv Rev* **181**, 114041 (2022).

22. Muntean, C. *et al.* Repositioning the over-the-counter antihistamine ebastine as an intracellular siRNA delivery enhancer. *Int J Pharm* 123348 (2023) doi:10.1016/j.ijpharm.2023.123348.

23. Bogaert, B. *et al.* A lipid nanoparticle platform for mRNA delivery through repurposing of cationic amphiphilic drugs. *Journal of Controlled Release* **350**, 256–270 (2022).

24. Kapoor, R., Peyear, T. A., Koeppe, R. E. & Andersen, O. S. Antidepressants are modifiers of lipid bilayer properties. *Journal of General Physiology* **151**, 342–356 (2019).

25. Schreier, S., Malheiros, S. V & de Paula, E. Surface active drugs: self-association and interaction with membranes and surfactants. Physicochemical and biological aspects. *Biochim Biophys Acta* **1508**, 210–34 (2000).

26. Britt, H. M., Prakash, A. S., Appleby, S., Mosely, J. A. & Sanderson, J. M. Lysis of membrane lipids promoted by small organic molecules: Reactivity depends on structure but not lipophilicity. *Sci Adv* **6**, eaaz8598 (2020).

27. Wheeler, K. E. *et al.* Environmental dimensions of the protein corona. *Nat Nanotechnol* **16**, 617–629 (2021).

28. Sebastiani, F. *et al.* Apolipoprotein E Binding Drives Structural and Compositional Rearrangement of mRNA-Containing Lipid Nanoparticles. *ACS Nano* **15**, 6709–6722 (2021).

29. Akinc, A. *et al.* Targeted delivery of RNAi therapeutics with endogenous and exogenous ligand-based mechanisms. *Molecular Therapy* **18**, 1357–1364 (2010).

30. Ramishetti, S. *et al.* A Combinatorial Library of Lipid Nanoparticles for RNA Delivery to Leukocytes. *Adv Mater* **32**, e1906128 (2020).

31. Semple, S. C. *et al.* Rational design of cationic lipids for siRNA delivery. *Nat Biotechnol* **28**, 172–176 (2010).

32. Love, K. T. *et al.* Lipid-like materials for low-dose, in vivo gene silencing. *Proc Natl Acad Sci U S A* **107**, 1864–1869 (2010).

33. Fenton, O. S. *et al.* Customizable Lipid Nanoparticle Materials for the Delivery of siRNAs and mRNAs. *Angewandte Chemie - International Edition* **57**, 13582–13586 (2018).

34. Whitehead, K. A. *et al.* Degradable lipid nanoparticles with predictable in vivo siRNA delivery activity. *Nat Commun* **5**, 4277 (2014).

35. Ni, H. *et al.* Piperazine-derived lipid nanoparticles deliver mRNA to immune cells in vivo. *Nature Communications 2022 13:1* **13**, 1–9 (2022).

36. Eygeris, Y., Patel, S., Jozic, A. & Sahay, G. Deconvoluting Lipid Nanoparticle Structure for Messenger RNA Delivery. *Nano Lett* **20**, 4543–4549 (2020).

37. Patel, S. *et al.* Naturally-occurring cholesterol analogues in lipid nanoparticles induce polymorphic shape and enhance intracellular delivery of mRNA. *Nat Commun* **11**, 983 (2020).

38. Paunovska, K. *et al.* Analyzing 2000 in vivo drug delivery data points reveals cholesterol structure impacts nanoparticle delivery. *ACS Nano* **12**, 8341–8349 (2018).

39. Dixon, A. S. *et al.* NanoLuc Complementation Reporter Optimized for Accurate Measurement of Protein Interactions in Cells. *ACS Chem Biol* **11**, 400–408 (2016).

40. Pottie, E., Tosh, D. K., Gao, Z. G., Jacobson, K. A. & Stove, C. P. Assessment of biased agonism at the A3 adenosine receptor using β-arrestin and miniGαi recruitment assays. *Biochem Pharmacol* **177**, 113934 (2020).

41. Pottie, E., Cannaert, A., Van Uytfanghe, K. & Stove, C. P. Setup of a Serotonin 2A Receptor (5-HT2AR) Bioassay: Demonstration of Its Applicability to Functionally Characterize Hallucinogenic New Psychoactive Substances and an Explanation Why 5-HT2AR Bioassays Are Not Suited for Universal Activity-Based Screening . *Anal Chem* **91**, 15444–15452 (2019).

42. Pottie, E., Cannaert, A. & Stove, C. P. In vitro structure–activity relationship determination of 30 psychedelic new psychoactive substances by means of β-arrestin 2 recruitment to the serotonin 2A receptor. *Arch Toxicol* **94**, 3449–3460 (2020).

43. De Backer, L., Cerrada, A., Pérez-Gil, J., De Smedt, S. C. & Raemdonck, K. Bio-inspired materials in drug delivery: Exploring the role of pulmonary surfactant in siRNA inhalation therapy. *Journal of Controlled Release* **220**, 642–650 (2015).

44. Guagliardo, R., Pérez-Gil, J., De Smedt, S. & Raemdonck, K. Pulmonary surfactant and drug delivery: Focusing on the role of surfactant proteins. *Journal of Controlled Release* **291**, 116–126 (2018).

45. Herman, L., De Smedt, S. C. & Raemdonck, K. Pulmonary surfactant as a versatile biomaterial to fight COVID-19. *Journal of Controlled Release* **342**, 170–188 (2022).

46. Shaffer, C. Mist begins to clear for lung delivery of RNA. *Nat Biotechnol* **38**, 1110–1112 (2020).

47. Zhang, H., Leal, J., Soto, M. R., Smyth, H. D. C. & Ghosh, D. Aerosolizable lipid nanoparticles for pulmonary delivery of mRNA through design of experiments. *Pharmaceutics* **12**, 1–16 (2020).

48. Kim, J. *et al.* Engineering Lipid Nanoparticles for Enhanced Intracellular Delivery of mRNA through Inhalation. *ACS Nano* **19**, 14792–14806 (2022).

49. Duncan, G. A., Jung, J., Hanes, J. & Suk, J. S. The Mucus Barrier to Inhaled Gene Therapy. *Molecular Therapy* **24**, 2043–2053 (2016).

50. Schneider, C. S. *et al.* Nanoparticles that do not adhere to mucus provide uniform and long-lasting drug delivery to airways following inhalation. *Sci Adv* **3**, e1601556 (2017).

51. Suk, J. S. *et al.* The penetration of fresh undiluted sputum expectorated by cystic fibrosis patients by non-adhesive polymer nanoparticles. *Biomaterials* **30**, 2591–2597 (2009).

52. Shaabani, E. *et al.* Increasing Angiogenesis Factors in Hypoxic Diabetic Wound Conditions by siRNA Delivery: Additive Effect of LbL-Gold Nanocarriers and Desloratadine-Induced Lysosomal Escape. *Int J Mol Sci* **22**, 9216 (2021).

53. Kopf, M., Schneider, C. & Nobs, S. P. The development and function of lung-resident macrophages and dendritic cells. *Nat Immunol* **16**, 36–44 (2015).

54. Baldassi, D. *et al.* Inhibition of SARS-CoV-2 replication in the lung with siRNA/VIPER polyplexes. *Journal of Controlled Release* **345**, 661 (2022).

55. Petithory, T. *et al.* Size-Dependent Internalization Efficiency of Macrophages from Adsorbed Nanoparticle-Based Monolayers. *Nanomaterials* **11**, 1963 (2021).

56. Pramanik, S. *et al.* Nanoparticle-Based Drug Delivery System: The Magic Bullet for the Treatment of Chronic Pulmonary Diseases. *Mol Pharm* **18**, 3671–3718 (2021).

57. Deshmane, S. L., Kremlev, S., Amini, S. & Sawaya, B. E. Monocyte chemoattractant protein-1 (MCP-1): An overview. *Journal of Interferon and Cytokine Research* **29**, 313–325 (2009).